Flood-induced load effects on real-scale structures: a 3D multilevel dynamic analysis

Umberto De Maio, Fabrizio Greco, Paolo Lonetti, Paolo Nevone Blasi, Girolamo Sgambitterra
Department of Civil Engineering, University of Calabria, Rende 87036 (CS), Italy
umberto.demaio@unical.it, https://orcid.org/0000-0002-7363-0738
fabrizio.greco@unical.it, https://orcid.org/0000-0001-9423-4964
paolo.lonetti@unical.it, https://orcid.org/0000-0003-0678-6860
paolo.nevoneblasi@unical.it, https://orcid.org/0000-0001-8807-2946
girolamo.sgambitterra@unical.it, https://orcid.org/0009-0003-8579-6844

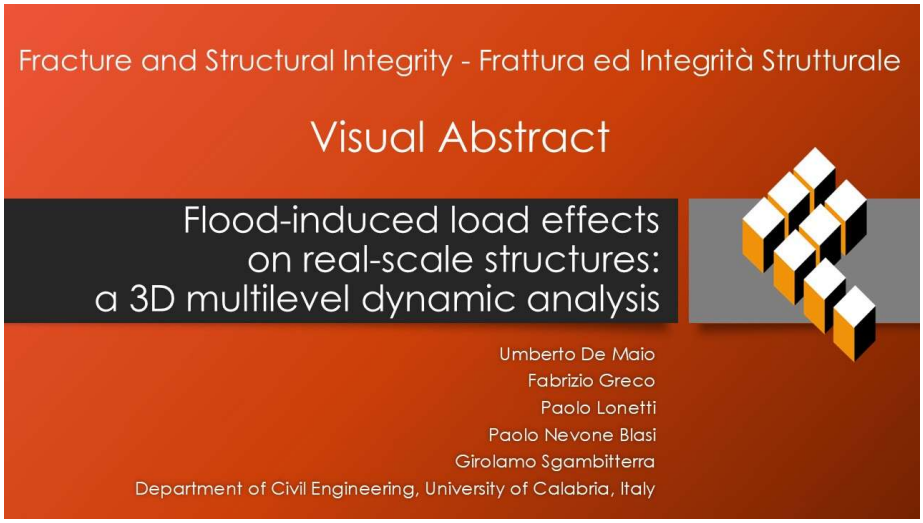

Citation: De Maio, U., Greco, F., Lonetti, P., Nevone Blasi, P., Sgambitterra, G., Flood-induced load effects on real-scale structures: a 3D multilevel dynamic analysis, Fracture and Structural integrity, 73 (2025) 59-73.

Received: 21.02.2025
Accepted: 30.04.2025
Published: 05.05.2025
Issue: 07.2025

KEYWORDS. Finite element analysis, Coupled damage-plasticity approach, Masonry structure, Flash floods.

INTRODUCTION

Flooding represents one of the most destructive environmental hazards, frequently triggered by extreme meteorological conditions like intense rain, storm surges, or snowmelt. The frequency and intensity of such events are increasing due to climate change, leading to significant impacts on both human lives and infrastructure. In particular, flash flood events are sudden and violent, causing catastrophic damage to buildings and the environment, especially in densely populated areas, posing a serious threat to human safety and the structural integrity of masonry buildings, particularly vulnerable to fluid hydrodynamic actions and sediment impacts during such events [1]. Due to the increasing frequency of such events, advanced methodologies to assess the structural vulnerability of buildings, under flooding, need to be developed. Available flood risk mitigation and structural vulnerability assessment strategies rely on indicator- and simulation-based methods.

Statistical approaches and vulnerability indicators are often employed, due to the advantages of an easy process and clarified vulnerability representation of a defined area. These approaches provide the commonly used vulnerability curves, damage matrices, and vulnerability indicators. In particular, the vulnerability curves are usually specific to the building type and link the intensity of a hazard to the expected damage or the cost of damage in relation to the total value at risk [2]. Damage matrices represent a qualitative method for vulnerability assessment. This method is not self-sufficient, as it relies on actual events to guide risk analysis or more in-depth assessments. Matrices are usually generated using empirical data or expert judgments: to the undamaged buildings are given a vulnerability value of 0, while fully damaged buildings receive a value of 1. Other buildings are classified into intermediate categories by an expert [3]. Vulnerability curves and matrices provide quantitative and semi-quantitative results, respectively, but usually tend to oversimplify the physical phenomena. As a matter of fact, these approaches exclusively focused on certain types of buildings, neglecting the specific characteristics of exposed elements, that contribute to their vulnerability. Moreover, an important limitation of these empirical approaches is that their reliability depends on both the quality and quantity of available empirical data; also, considering the continuous evolution of the built environment and human activities, these empirical methods have some "historical limitations" [4]. As a result, neither curves nor matrices are adequate to provide useful guidance on how to reduce risks. On the other hand, vulnerability indicators are measurable variables or operational representations of physical, technical, social, and economic characteristics that reflect the ability of a structure or system to resist, respond, and adapt to the effects of hydraulic events, such as flooding or inundation. These indicators help to quantify the probability of structural damage or degradation following such an event. In the literature, several studies, able to link the physical vulnerability of buildings to their specific characteristics by means of vulnerability indicators, have been carried out in the context of mountain hazards [5]. In particular, different databases are generated to classify the building characteristics considered significant in assessing their susceptibility to hazard events, such as landslides, floods or tsunamis and damage. To each of these characteristics (indicators) was assigned a weight, determined by their perceived importance through expert evaluation, and then aggregated to estimate the physical vulnerability of individual buildings. This methodology is not based on empirical data and, for this reason, can be applied in the absence of such data and even in areas without event records. However, vulnerability indicators have issues such as data availability and uncertainties in their selection, standardization, weighting, and aggregate. Neglecting process intensity is a major drawback that might cause discrepancies between assigned vulnerability indices and real losses. Additionally, these methodologies often require highly detailed, building-specific data, which can only be obtained through time-intensive field surveys.

In contrast to indicator-based approaches, simulation-based methods provide a more explicit representation of the physical mechanism of the hazard and the consequent damage affecting the impacted structures, thus rendering the results more adaptable to vulnerability assessment. As a matter of fact, different physical model-based methods, including scenario analyses, have been proposed in the past decade. They mainly focus on the mechanical response of the structures subjected to specific hazard scenarios and the damage process, offering a more detailed understanding of potential vulnerabilities [6]. The growing popularity of these methods derives from their ability to provide targeted indications that support more accurate risk assessment and more effective mitigation strategies than traditional, generalized methods. Earlier studies of building vulnerability using numerical models have been based on both empirical and structural approaches. Empirical models provide statistical correlations using available flood intensity data derived from past hazard events, while structural models analyze the physical response of buildings under hydraulic pressure. This hybrid methodology allows rough evaluations of structural vulnerability to be predicted. For example, a simplified conceptual scheme to quantify the vulnerability of buildings exposed to torrent processes is proposed by [7]. Three different steps are introduced: i) hazard intensity computation, through 2D flow inundation modeling; ii) impact analysis of debris/water flow on the structure; iii) physical response of the building by Finite Element (FE) analysis. A more complex vulnerability scheme is proposed instead by [8] developing a coupled probabilistic-physical model to assess the structural vulnerability under flood events. In particular, the building is considered by a set of structural/non-structural components, whose stiffness is affected by damage induced by hydrodynamic pressure and contact between water and structural materials. Detailed numerical modeling of water infiltration is carried out using engineering models in order to obtain a complete assessment of damage and stiffness reduction. Since this method is based on conditional probabilities, it can be used with numerous types of buildings. The limit analysis theory is employed in [9] to analyze the stability of masonry walls, subjected to flooding in different structural configurations, and dimensionless vulnerability thresholds, based on wall aspect ratios in terms of geometry properties, are provided. This analytical framework, validated using FEM models, provides the maximum admissible load and the consequent structural damage as a function of specific building characteristics, thus offering useful support for risk management in both scientific and operative contexts. However, the analytical model adopts simplified fluid action considering the hydrodynamic pressure only by means of an equivalent pseudo-static formulation as a function of the fluid's velocity and density with an amplification factor, neglecting the dynamic effects produced by the extensive momentum

exchange process in the early stage of the impact. Therefore, it is not derived from a temporal analysis. Recently, several studies have focused on the fluid-structure interaction modeling simultaneously the fluid flow and structural response [10]. In particular, in these works, fluid and structural systems are coupled by the Arbitrary Lagrangian-Eulerian (ALE) methodology, thus allowing the fluid motion, fluid/structure interface and path-following nature of the applied loads on the structure to be correctly simulated. As a matter of fact, the structural response strongly depends on the hydrodynamic forces, and, at the same time, the fluid domain is influenced by the structural deformations, obtaining moving wall boundary conditions with displacement and speed fields coinciding with those of the structural system [11]. The assessment of masonry structures subjected to extreme loads, such as flooding, can benefit from methodologies developed for analyzing the collapse mechanisms of reinforced masonry arches and historical structures. Studies on limit analysis and numerical modeling of FRP-strengthened masonry arches provide valuable insights into structural stability, accounting for material non-linearity, frictional sliding, and failure mechanisms under external forces [12–15]. Additionally, visual programming techniques for evaluating out-of-plane failure in masonry buildings introduce efficient computational tools that can be adapted to assess hydrodynamic-induced structural damage in flood scenarios [16]. These approaches enhance the accuracy of vulnerability assessments by integrating numerical simulations with optimization-based structural analysis. Advanced theoretical and numerical approaches provide valuable insights into the structural response of masonry buildings under extreme hydrodynamic loads. Studies on the buckling behavior of shear-deformable nanobeams using nonlocal elasticity theory help understand stability and local instabilities in masonry walls under fluid pressure [17]. Additionally, boundary-layer corrections for stress and strain distributions in heterogeneous media highlight the role of material inhomogeneities near structural discontinuities, crucial for assessing damage evolution in flood-exposed masonry structures [18]. These contributions emphasize the importance of multi-scale and nonlocal modeling in structural vulnerability analysis. Regarding the structural response, in terms of load-carrying capacity and failure mechanisms, appropriate strength criterion and damage models are employed. An anisotropic brittle damage model, available in the literature, able to simulate the progressive degradation of tensile and shear strengths across smeared cracks initiated under tensile/compressive loads, is adopted for masonry material in [19]. Instead, in [10] the damage description for a failure mechanism is defined as the ratio between the demand and capacity quantities, indicating how a single element of the structural system is far or close to the unsafety condition. The combination of the ALE formulation and damage models allows a detailed description of the interaction between flash floods and masonry structures in the typical simulation scenarios, as well as providing the main characteristics of structural failure.

Despite significant efforts in analyzing the physical vulnerability of structures exposed to flooding events, the real physics of these phenomena still needs to be clarified. In particular, the assessment of masonry structures subjected to flash floods is in its early stages, with many aspects yet to be fully explored. To address this knowledge gap, this study introduces a novel 3D multilevel framework, able to analyze the flood-induced load effects on masonry structures. The proposed model integrates the computational fluid dynamic with a coupled structural damage-plasticity model, offering a more robust tool for understanding the vulnerability of masonry buildings to extreme flooding events. Detailed simulations of the mechanical behavior of buildings subjected to hydrodynamic action are performed, and the associated loading curves and damage patterns are predicted. Finally, a parametric study to assess the influence on the structural response of fluid flow properties, in terms of water depth and inlet velocity, is carried out.

THEORETICAL FORMULATION AND NUMERICAL IMPLEMENTATION OF THE MULTILEVEL MODEL

The core idea of the proposed 3D numerical framework relies on the combination of two work scales: a macro-scale domain is adopted to simulate the fluid flow impacting a rigid solid, while a meso-scale domain is employed to assess the structural response of a building subjected to hydrodynamic actions, in terms of load-carrying capacity and damage patterns. The two models interact in a one-way coupling scheme. In particular, from the macro-scale simulation a fluid pressure function is extracted, encapsulating the spatial and temporal distribution of pressures on the surfaces of the rigid solid, representing the building. This function, which includes point-wise pressure values on the walls of the building at each time step, is then provided to the meso-scale model. The meso-scale model uses this pressure function as a dynamic load to evaluate the nonlinear structural response of the building. Structural components, such as walls and slabs, are analyzed under time-dependent pressure loads, to assess their damage patterns and load-carrying capacity. The two models operate synchronously, with the macro-scale model updating the pressure function at each time step, which is subsequently applied to the meso-scale model. This iterative procedure ensures that the evolving hydrodynamic forces are consistently accounted in the structural analysis. The workflow, as illustrated in Fig. 1, highlights the unidirectional interaction and the integration between the fluid flow and the structural mechanics domains. From a computational point of view, the fluid

flow in the macro-scale analysis is simulated by using the computational fluid dynamic (CFD) methodology, while the nonlinear structural behavior of the building is described by a coupled structural damage-plasticity model (CDP), both available within the commercial software COMSOL Multiphysics. It should be noted that the proposed structural model, based on a coupled damage-plasticity approach, assumes masonry as a homogeneous material and, therefore, does not explicitly capture the preferential crack paths that may develop along mortar joints. This modeling choice, although representing a simplification of the real heterogeneous nature of masonry, enables the prediction of the areas most prone to damage and provides valuable information regarding the extent and distribution of structural degradation under flood-induced actions. Moreover, the analysis is primarily calibrated for masonry structures of good mechanical quality. While the results are expected to be reliable for well-constructed masonry walls, caution must be exercised when extending the conclusions to historical buildings or degraded structures, where local failure mechanisms, such as out-of-plane overturning or partial collapses, are more frequent due to material deterioration, inadequate construction techniques, and poor mechanical connections. Nevertheless, it is worth mentioning that local failure mechanisms may also occur in modern masonry structures, depending on their geometric and constructional characteristics.
In the following sections, the theoretical approaches of the macro and meso-scale models are briefly explained, together with some numerical implementation details.

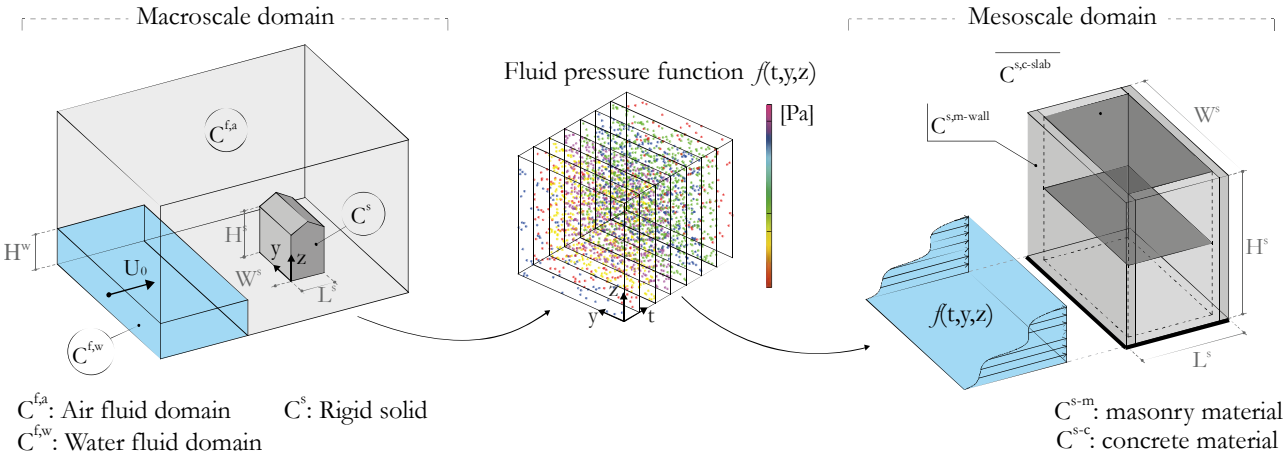

Figure 1: Workflow of the proposed multilevel numerical framework.

Macro-scale model for fluid flow simulation

The free-stream fluid flow and its impact on rigid solids is simulated in the macro-scale domain by using the *k-ε* turbulence model proposed by [20]. It is based on the Reynolds-averaged Navier-Stokes (RANS) equations, written for an incompressible (constant density ρ) and Newtonian fluid, able to describe turbulent flows by focusing on the averaged motion of the fluid, making them widely applicable in engineering and computational fluid dynamics (CFD). The continuity and momentum equations are expressed in the following forms:

$$\rho\frac{\partial \overline{u}_i}{\partial x_i}=0$$
$$\rho\frac{\partial \overline{u}_i}{\partial t}+\rho\overline{u}_j\frac{\partial \overline{u}_i}{\partial x_j}=-\frac{\partial \overline{p}}{\partial x_i}+\mu\frac{\partial^2 \overline{u}_i}{\partial x_j^2}-\frac{\partial \overline{u_i' u_j'}}{\partial x_j}+\overline{f}_i \quad (1)$$

were $\overline{u}_i$ and $\overline{p}$ are the time-averaged velocity components and pressure, respectively, while μ is a fluid property associated with the kinematic viscosity and $\overline{u_i' u_j'}$ is the Reynolds stress tensor representing the effect of turbulence on the flow. The volume force vector is $\overline{f}_i$. The inclusion of the Reynolds stress tensor introduces a closure problem, as it adds more unknowns than the number of equations. The adopted *k-ε* model provides a framework for solving the RANS equations by approximating the effects of turbulence through additional transport equations for two dependent variables, i.e., the turbulent kinetic energy, *k*, representing the energy contained in the turbulent flow, which is a measure of the intensity of

turbulence in the flow, and the turbulent dissipation rate, ε, which quantifies the rate at which the turbulent kinetic energy (k) is dissipated into thermal energy due to the viscous effects . The transport equations for k and ε read, respectively:

$$\begin{aligned}\rho\frac{\partial k}{\partial t}+\rho\overline{u}_i\frac{\partial k}{\partial x_i}&=\frac{\partial}{\partial x_j}\left(\frac{\mu_t}{\sigma_k}\frac{\partial k}{\partial x_j}\right)+P_k-\rho\varepsilon\\ \rho\frac{\partial \varepsilon}{\partial t}+\rho\overline{u}_i\frac{\partial \varepsilon}{\partial x_i}&=\frac{\partial}{\partial x_j}\left(\frac{\mu_t}{\sigma_\varepsilon}\frac{\partial \varepsilon}{\partial x_j}\right)+C_{\varepsilon 1}\frac{\varepsilon}{k}P_k-C_{\varepsilon 2}\rho\frac{\varepsilon^2}{k}\end{aligned} \tag{2}$$

where P_k represents the production of turbulent kinetic energy due to the mean flow gradients and quantifies how much energy from the mean flow is transferred into turbulence through shear or strain in the flow, μ_t is the turbulent viscosity and expressed by the following form:

$$\mu_t=\rho C_\mu\frac{k^2}{\varepsilon} \tag{3}$$

Eqns. (2) and (3) also consist of some empirical constants, i.e., σ_k, σ_ε, $C_{\varepsilon 1}$, $C_{\varepsilon 2}$, and C_μ whose values have been obtained by a combination of theoretical analysis, calibration, and experimental data fitting [21].
To track the evolution of the interface between the two different fluid flows, air and water, a level set method is employed, able to represent the interface implicitly through a continuous function ϕ defined over the computational domain. The method adds the following equation, called level set function:

$$\frac{\partial \phi}{\partial t}+u_i\frac{\partial \phi}{\partial x_i}=\gamma\frac{\partial}{\partial x_i}\left(\varepsilon\frac{\partial \phi}{\partial x_i}-\phi(1-\phi)\frac{\frac{\partial \phi}{\partial x_i}}{\sqrt{\frac{\partial \phi}{\partial x_j}\frac{\partial \phi}{\partial x_j}}}\right) \tag{4}$$

where γ is the reinitialization parameter, and ε is the numerical interface thickness controlling parameter set proportional to the maximum finite element size in the component. The density is a function of the level set function. If ρ_1 and ρ_2 are the constant densities of water and air, respectively, water corresponds to the domain where $\phi < 0.5$, and air corresponds to the domain where $\phi > 0.5$.

Meso-scale model for structural response simulation

The proposed numerical framework relies on a coupled damage-plasticity model, proposed by [22], to investigate the structural response of buildings subjected to flash floods. With respect to available discrete fracture models based on cohesive approach [11,23–25], the model combines damage mechanics and plasticity theory for an accurate description of the mechanical behavior of the material under various loading conditions, capturing both softening behavior due to the tensile cracking and the inelastic deformations caused by compressive stress. The theoretical framework is based on the following constitutive equations:

$$\begin{aligned}\boldsymbol{\sigma}&=(1-d_t)\boldsymbol{\sigma}_{un}^{+}+(1-d_c)\boldsymbol{\sigma}_{un}^{-}\\ \boldsymbol{\sigma}_{un}&=\boldsymbol{C}_e:(\boldsymbol{\varepsilon}-\boldsymbol{\varepsilon}_p)\end{aligned} \tag{5}$$

according to which the current stress tensor $\boldsymbol{\sigma}$ depends on the positive and negative part of the effective stress tensor $\boldsymbol{\sigma}_{un}$ obtained by a spectral decomposition in order to account for the different mechanical responses of masonry under tensile and compressive loading conditions and reduced by the isotropic damage variables d_t and d_c in tension and compression

states, respectively. The effective stress tensor, depending on the elastic stiffness tensor $\boldsymbol{C}_e$ and strain tensor $\boldsymbol{\varepsilon}$, takes into account the residual plastic deformations through the plastic strain tensor $\boldsymbol{\varepsilon}_p$. The plastic model uses a yield function $f_p\left(\boldsymbol{\sigma}_{un},\boldsymbol{\kappa}_p\right)$, a plastic potential $Q_p\left(\boldsymbol{\sigma}_{un},\boldsymbol{\kappa}_p\right)$, governing the direction of the plastic flow, and a plastic multiplier $\dot{\lambda}_p$, to define the following flow rule:

$$\dot{\boldsymbol{\varepsilon}}_p = \dot{\lambda}_p \frac{\partial Q_p\left(\boldsymbol{\sigma}_{un},\boldsymbol{\kappa}_p\right)}{\partial \boldsymbol{\sigma}_{un}} \tag{6}$$

where $\boldsymbol{\kappa}_p$ is the scalar hardening variable describing how the yield surface changes during plastic loading. The well-known Kuhn-Tucker conditions regulate the activation of plasticity, ensuring that plastic deformation occurs only when the material state lies on the yield surface. These conditions are expressed as:

$$f_p \le 0, \quad \dot{\lambda}_p \ge 0, \quad \dot{\lambda}_p f_p = 0 \tag{7}$$

A detailed description of the individual components of the plastic model are discussed in [22].
On the other hand, the damage model, as reported in Eq. 5, employes two distinct damage variables d_t and d_c, and their evolution is governed by the following damage loading function f_{d_i}:

$$f_{d_i} = \varepsilon_{eq_i}\left(\boldsymbol{\sigma}_{un}\right) - \boldsymbol{\kappa}_{d_i} \qquad i = [t,c] \tag{8}$$

where ε_{eq} is the equivalent strain, identical for both tensile and compression state, and it is a scalar quantity derived from the plastic yield surface $f_p = 0$, while $\boldsymbol{\kappa}_d$ is a history variable representing the maximum equivalent strain recorded over time, ensuring that the material retains a memory of prior loading. Moreover, the damage evolves irreversibly according to the Kuhn-Tucker conditions, which are defined as:

$$f_{d_i} \le 0, \quad \dot{\boldsymbol{\kappa}}_{d_i} \ge 0, \quad \dot{\boldsymbol{\kappa}}_{d_i} f_{d_i} = 0 \tag{9}$$

Subsequently, the damage variables are defined on the form:

$$d_i = g_{d_i}\left(\boldsymbol{\kappa}_{d_i}, \boldsymbol{\kappa}_{d_i 1}, \boldsymbol{\kappa}_{d_i 2}\right) \tag{10}$$

where g_d is a function for describing the evolution of damage in terms of the primary history variable $\boldsymbol{\kappa}_d$ and additional history variables $\boldsymbol{\kappa}_{d1}$ and $\boldsymbol{\kappa}_{d2}$. These additional variables allow for a more detailed representation of complex phenomena, such as strain hardening or nonlinear damage evolution. The above-explained formulation is particularly suited for quasi-brittle materials like concrete or masonry, where the interaction between damage and plasticity plays a crucial role in determining mechanical performance under tension and compression states. The integration of multiple damage and plasticity components ensures that the model can accurately replicate both microcracking-induced degradation and plastic flow mechanisms. Furthermore, it must be highlighted that the present study neglects possible slip between masonry elements, potential scour effects at the foundation level, and material degradation due to prolonged contact with water. These aspects represent further limitations of the proposed approach and will be addressed in future research developments.

APPLICATION OF THE PROPOSED MULTILEVEL FRAMEWORK TO A MASONRY BUILDING

In this section, the 3D numerical framework, explained in the previous section, is employed to investigate the structural behavior of a masonry building subjected to flash flood loading conditions, previously analyzed with a 2D model by [10]. The section begins by illustrating the material properties, as well as the geometric and boundary conditions, of the

entire numerical domain, including fluids (i.e. water and air) and the masonry structure. It concludes with a discussion of the numerical results obtained by the macro- and meso-scale analyses.

Geometric, materials and computational details

The proposed model incorporates a multilevel approach, where the fluid propagation and its impact forces are analyzed at the macro-scale, while the structural response, including damage evolution, is simulated at the meso-scale. This coupled environment ensures a comprehensive representation of the fluid-structure interaction, capturing both the global behavior of the flood and the localized effects on the structure. The geometric and boundary conditions of both macro- and meso-scale domains are reported in Fig. 2. In particular, in the macro-scale domain, the fluid flow, with prescribed constant velocity U_0, discharging from an inlet wall which is 5 meters wide (matching the width of the structure) and H^w height, is simulated to obtain the hydrodynamic pressure acting on the adjacent structure. On the external walls of the macro-scale environment (highlighted with blue contours in Fig. 2), except for the bottom wall representing the ground, outlet conditions are imposed by prescribing the averaged total pressure equal to 0 in the weak forms, thus allowing a net outflow from the domain. The structure is here modeled as a rigid solid, therefore the effects of structural deformation on the fluid distribution over the solid during its motion are not accounted for. In the meso-scale environment, the structure is no longer modeled as a rigid solid but rather as a system of individual components governed by prescribed constitutive laws. Specifically, the building's walls are modeled by 0.4 m thick masonry brick elements exhibiting nonlinear mechanical behavior (described in the previous section), while linearly elastic shell elements are employed for floor and roof slabs.

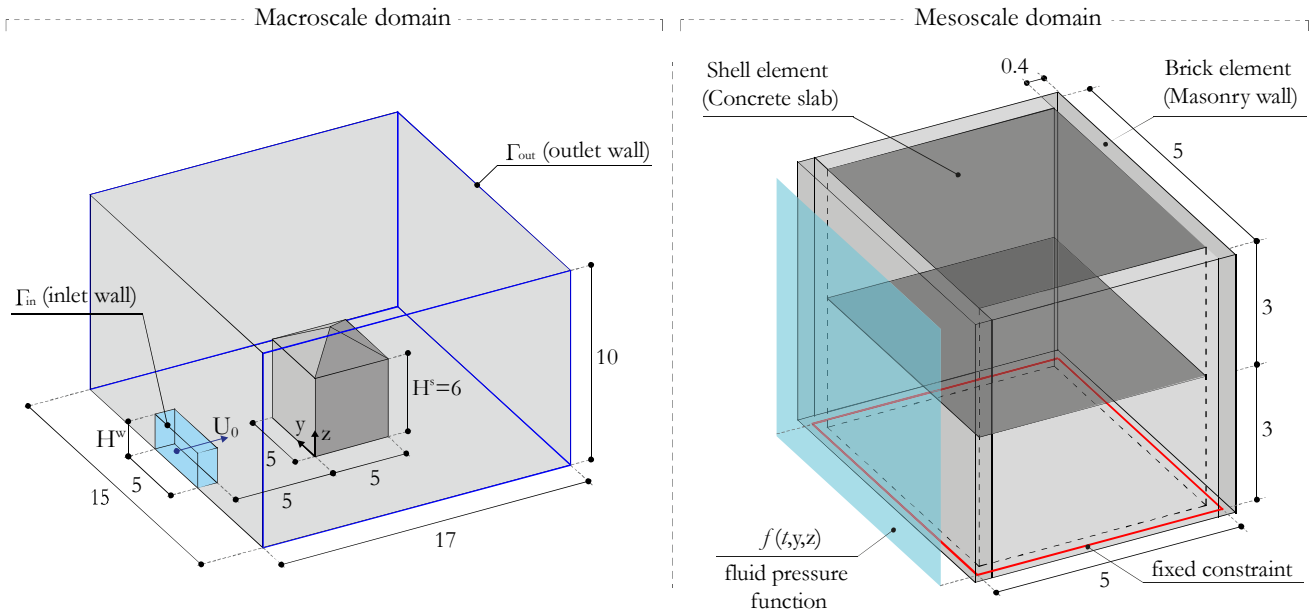

Figure 2: Geometric and boundary conditions of the simulated 3D numerical environment in the macro- and meso-scale analysis. The measurements are expressed in meters (m).

The adopted materials properties are summarized in Tab. 1.

Structural element	Density [kg/m³]	Young's modulus [MPa]	Poisson ratio	Compressive strength [MPa]	Tensile strength [MPa]	Fracture energy [N/m]
Wall	1800	3000	0.2	3	0.035	0.055
Slab	2400	20000	0.25	-	-	-

Table 1: Mechanical properties adopted for walls and slabs constituting the simulated structure.

In the meso-scale model, the vertical loads acting on the masonry walls include both the self-weight of the walls and the additional loads transmitted by the floor systems. The contribution of the floors was modeled by considering the tributary area associated with each floor slab, thereby ensuring a realistic distribution of stress field consistent with the structural configuration of a real-scale building.

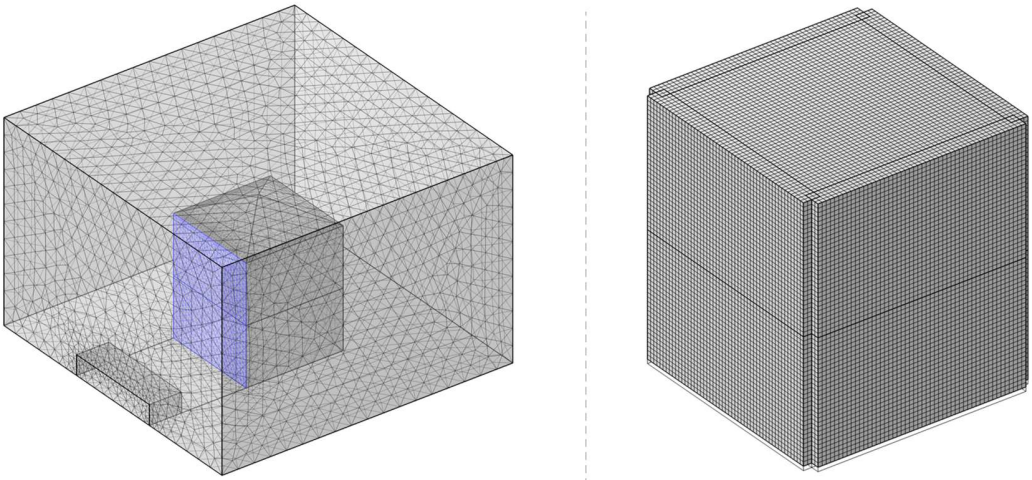

(a) (b)

Figure 3: Computational discretization adopted for the macro-scale (a) and meso-scale (b) analyses.

In order to reduce the computational efforts of the meso-scale analysis, only the pressure recorded on the frontal wall of the rigid solid in the macro-scale domain, which faces the inlet of the fluid, is considered as a dynamic load on the structure. Similarly, to further minimize computational costs, the nonlinear damage process is only investigated in the wall affected by the hydrodynamic pressure. A perfect adhesion is adopted between the walls and slabs for the structure. A fixed constraint is prescribed along the bottom face of the masonry brick elements. The macro-scale computational domain is discretized with free tetrahedral elements by imposing a maximum size equal to 0.6 m (see Fig. 3a). A mesh refinement is performed to the surface of the rigid solid positioned directly in front of the fluid inlet to ensure an accurate evaluation of the hydrodynamic pressure. This surface (highlighted in blue color in Fig. 3a) is discretized by imposing a maximum element size equal to 0.2 m. On the other hand, the computation mesh of the meso-scale domain, depicted in Fig. 3b, consists of free quad elements arranged by a structured tessellation with a maximum element size equal to 0.1 m. A time-dependent solver with phase initialization, available in COMSOL Multiphysics, is employed to perform the macro-scale numerical analysis. This solver is particularly suited for two-phase flow models and involves two key steps: phase initialization and time-dependent analysis. During phase initialization, the solver computes the reciprocal distance to the phase interface which establishes precise initial conditions for future time-dependent simulations. During the time-dependent step, the solver applies the Backward Differentiation Formula (BDF) for implicit time integration alongside adaptive time-stepping which delivers both stability and efficiency. A time-dependent solver, but with the generalized-α method, is employed for structural response simulations at the meso-scale level. The implicit second-order accurate method provides an optimal trade-off of precision and stability which makes it appropriate for dynamic simulations that require minimal numerical damping.

Macro-scale results

The numerical results obtained by the macroscale analysis, considering the water depth and inlet velocity equal to $H''' = 1$ m and $U_0 = 5$ m/s respectively, are reported and discussed here. In particular, Fig. 4 illustrates the temporal and spatial evolution of the pressure recorded along the frontal wall surface of the rigid solid (see Fig. 2a). In Fig. 4a, the pressure curve as a function of time, with three red-marked characteristic points (A, B, and C) signifying the beginning of three fluid-structure interaction stages, is depicted. During the pre-impact phase represented by Point A, the structure remains untouched by the fluid. The detected low pressure at this stage results from the compression of air which moves in front of the incoming fluid. The peak load stage is represented by point B which happens right when the fluid makes contact with the structure because of its high speed at that instant. Point C represents the stabilized flow phase as evidenced by the pressure reaching a steady level which shows that the system has achieved a quasi-steady state.

In Fig. 4b, the pressure distribution from the present model is compared with other approaches, including the quasi-static approximation and the 2D model developed by Lonetti et al. [10]. The pressure envelope considers the range of pressure values during the simulation, highlighting the pressure curve (blue line) predicted at the peak load (Point B of Fig. 4a).

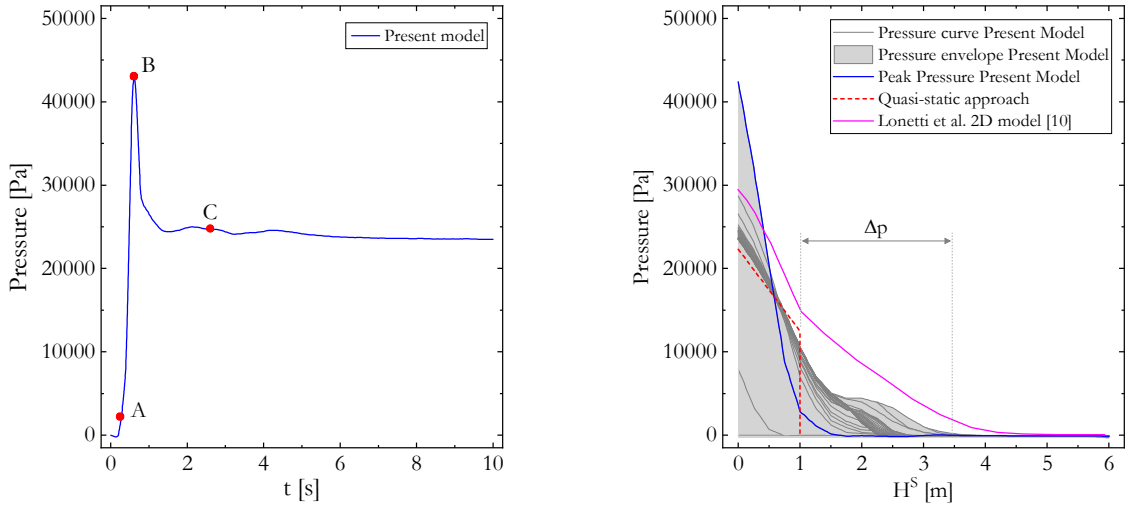

Figure 4: Maximum pressure (a) and pressure envelope (b) acting on the selected wall.

Globally, the static approximation and the proposed model predict a similar pressure distribution along the structure, with notable differences, in particular, the peak load, which is higher in the computational model due to the transient effects of fluid impact and the fluid-structure interaction zone, which is greater in the dynamic model. The quasi-static approach is based on the following formula considering both hydrostatic and hydrodynamic components:

$$p_{approx} = \frac{1}{2}\rho g H^{w} + \frac{1}{2} C_D \rho \left(U_0\right)^2 \tag{11}$$

where ρ is the fluid density, g is the gravitational acceleration, H^{w} is the water depth, U_0 is the fluid velocity, and C_D is a dynamic coefficient chosen equal to 1. The difference in the pressure fluid impact region, highlighted with Δp in Fig. 4b, between the static and computational predictions emphasizes the limitations of the static approximation. In particular, the quasi-static approach underestimates the pressure height compared to the present dynamic model, as it is limited to the imposed water depth of $H^{w} = 1$ m, highlighting the importance of considering transient effects to accurately capture the actual pressure distribution and structural response under fluid impact.

The evolution of fluid flow within the 3D framework, together with its interaction with the rigid solid, at 3 different timesteps (Point A, B and C reported in Fig. 4a), is presented in Fig. 5. The values of the level set function ϕ (described in the previous Section) are reported in the middle column of the figure in order to detect the volume fractions of water and air. The presented visualization depicts the values of ϕ recorded in the central plane of the fluid domain, indicated by the red bounding box in the leftmost column. The right column visualizes the pressure maps induced by fluid across the surface frontal to fluid inlet, highlighted with a green bounding box in the leftmost column.

At point A, no direct contact between water and the solid is recorded yet. At point B, during the peak load phase, both function ϕ and pressure reach their maximum values, reflecting the initial, sudden fluid/solid interaction. By point C, the distribution has stabilized, and the pressure map indicates a quasi-constant value along the fluid/solid contact zone, suggesting that the system has achieved a steady state. In light of the results obtained, the present model demonstrates powerful capabilities for precisely simulating fluid motion alongside rigid body interactions within a complete three-dimensional space. The simulation effectively represents the fluid's dynamic behavior through its initial impact stage followed by flow development and concluding with stabilization. The pressure curve in Fig. 4a shows that peak pressure reaches its maximum at the moment of impact which demonstrates the high speed and momentum of the incoming fluid. The maximum pressure point leads to a gradual decline until it reaches a stable lower pressure level which represents a quasi-steady state where the load from the fluid on the structure becomes consistent.

Meso-scale results

The meso-scale analysis focuses on the structural response to the fluid pressure extracted from the macro-scale simulation. Unlike the macro-scale approach, which treats the structure as a rigid solid, this analysis accounts for the elastic and fracture

properties of the constituent materials, specifically masonry and concrete. As described in the previous section, this modeling approach enables a more realistic evaluation of the mechanical behavior of the structure, capturing its deformation and potential failure mechanisms under fluid impact.

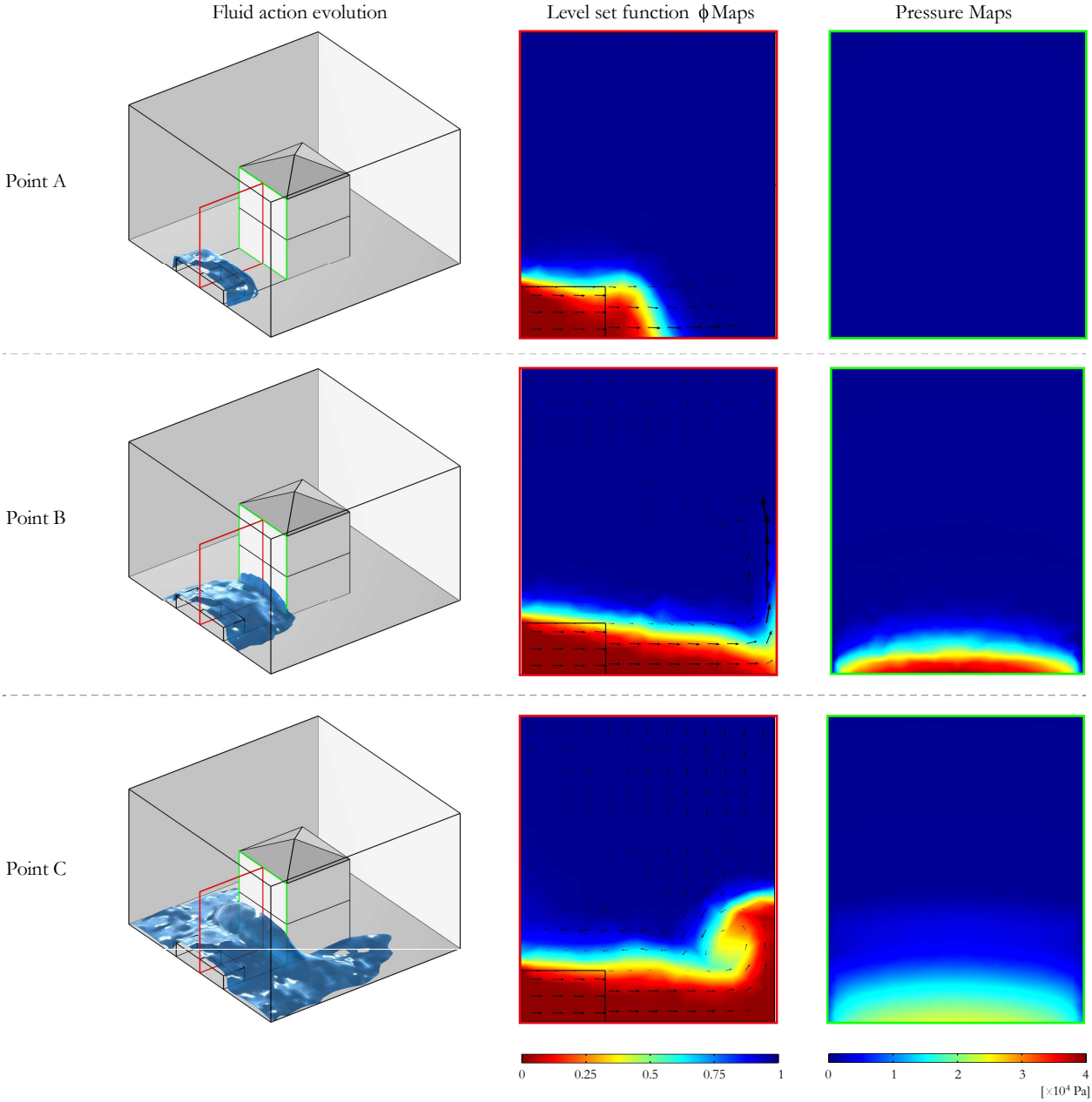

Figure 5: Density of fluids (water and air) and pressure distribution predicted by the macroscale model.

The structural response predicted by the meso-scale model, in terms of load and displacement, is reported in Fig. 6. As shown in Fig. 6a, the loading curve exhibits the same trend observed in the macro-scale analysis (Fig. 4a), as expected since the hydrodynamic pressure field extracted from the macro-scale simulation is directly applied as a time-dependent load in the meso-scale model. This result confirms the correct transfer and implementation of the fluid-induced actions within the proposed multiscale framework. For comparison purposes, a simulation considering a quasi-static loading condition obtained by Eqn. 11, is performed. The comparison between the obtained results highlights that the load predicted by the proposed model approaches the quasi-static model only when the stabilized flow condition is reached, with a percentage difference of approximately 11% in the load value. The static fluid load expression provided by standard codes yields a more conservative estimation compared to the dynamic model, as it does not account for the transient effects of the initial impact

phase, where significantly higher peak load values are observed. In Fig. 6b, the maximum out-of-plane displacement of the structure is reported over time. After the peak load, the dynamic response shows an immediate significant displacement growth with smaller oscillations until a stabilized deformation is reached. It is worth noting that the quasi-static approach leads to an underestimation of maximum displacement of about 28% because it fails to account for peak load effects which underscores the need to include dynamic fluid-structure interactions in structural assessments.

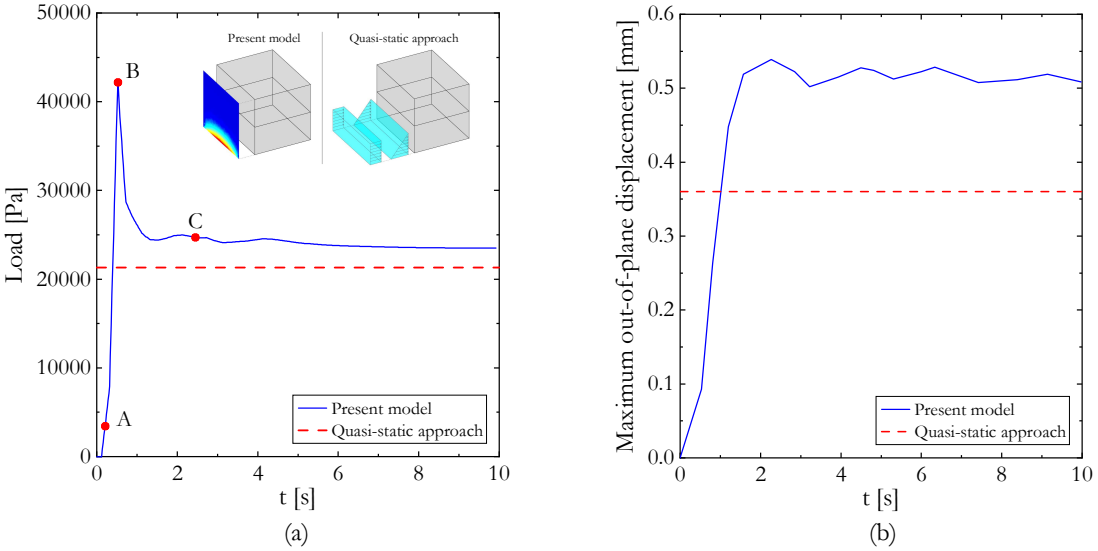

Figure 6: Maximum load (a) and out-of-plane displacement (b) curves predicted by the meso-scale model.

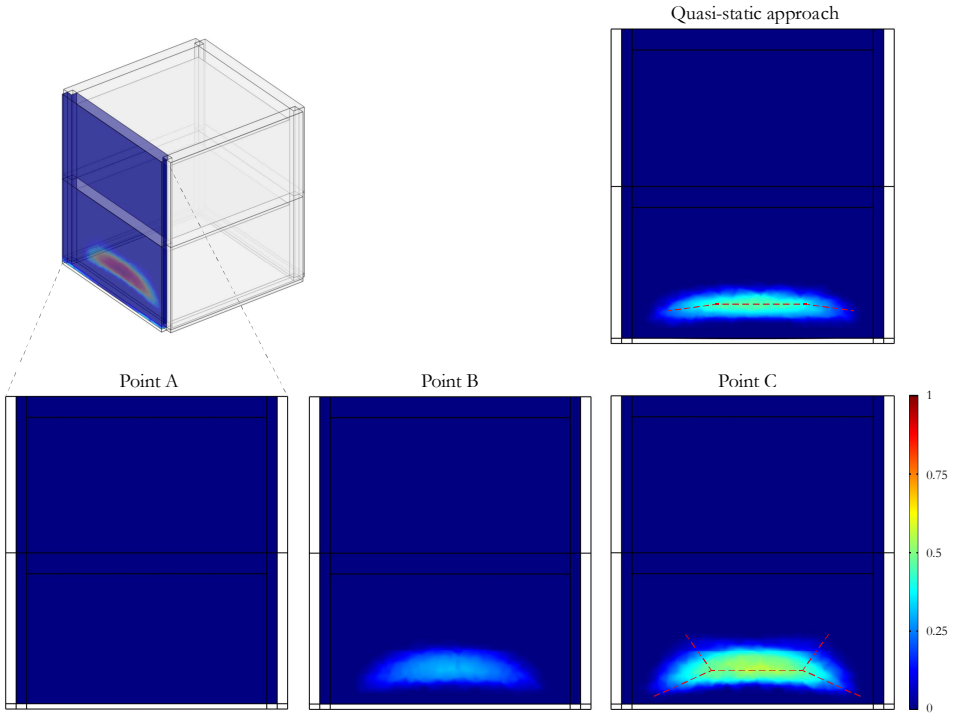

Figure 7: Damage maps predicted by the meso-scale model.

Fig. 7 shows the damage maps of the wall most affected by the fluid action at three different time steps, corresponding to points A, B, and C highlighted in the loading curve of Fig. 6a. Analysis reveals that structural damage reaches its highest value of approximately 0.62 during the period when the fluid flow stabilizes (Point C) rather than at the moment of peak pressure (Point B). Structural damage continues to increase because of the progressive fluid load application even following the peak pressure stage. Furthermore, the damage pattern observed in the numerical model closely follows the expected

failure mode of a masonry wall with hinged supports at its edges. Damage bands extend from the wall center toward its edges which demonstrate the common failure patterns identified in experimental and numerical research on masonry structures subjected to lateral forces. On the right side of Fig. 7, a comparison with the quasi-static approach is presented. The static model provides a less realistic damage distribution, showing a localized damaged area at the height of the resultant fluid force rather than the expected distributed failure mechanism. Finally, we can state that the dynamic effects play a crucial role in determining the realistic damage evolution of the structure, highlighting the limitations of static approaches in capturing the actual structural response under hydrodynamic loads.

Parametric analysis: influence of water depth and inlet velocity on the global structural response

A parametric study was performed to investigate the influence of water depth and velocity on the global structural response of the real-scale structure using the proposed multilevel model. The analysis was conducted by systematically varying the water depth from 1 to 3 m ($H^w = 1, 2, 3$ m) and the fluid velocity from 1 to 5 m/s $U_0 = 1, 3, 5$ m/s, allowing for a deeper understanding of the fluid-structure interaction under different impact conditions. The structural response was evaluated in terms of load-carrying capacity, maximum out-of-plane displacement, and damage pattern, comparing the dynamic model with the quasi-static approach.

Fig. 8 presents the results of parametric analysis. In particular, the plots illustrate the load curve (blue lines) and the maximum out-of-plane displacement (red lines) for different combinations of water depth and inlet velocity. Each row corresponds to a specific water depth, while the three columns represent increasing fluid velocity. The results from the present dynamic model are compared with the quasi-static approach (dashed lines), providing insight into the role of transient effects in fluid-induced loading conditions. Additionally, damage maps recorded at the stabilized flow condition are shown in the inset images for each case. The comparison between the dynamic and quasi-static approaches highlights significant differences. At low water depth $H^w = 1$ m, the quasi-static and dynamic models predict similar load distributions, and the damage remains localized at the lower portion of the wall. As the fluid velocity and water depth increase $U_0 = 5$ m/s, the peak load in the dynamic model becomes significantly higher than in the quasi-static approach, confirming the importance of accounting for impact dynamics. The quasi-static model consistently underestimates both the peak pressure and the maximum displacement, failing to capture the real transient response of the structure.

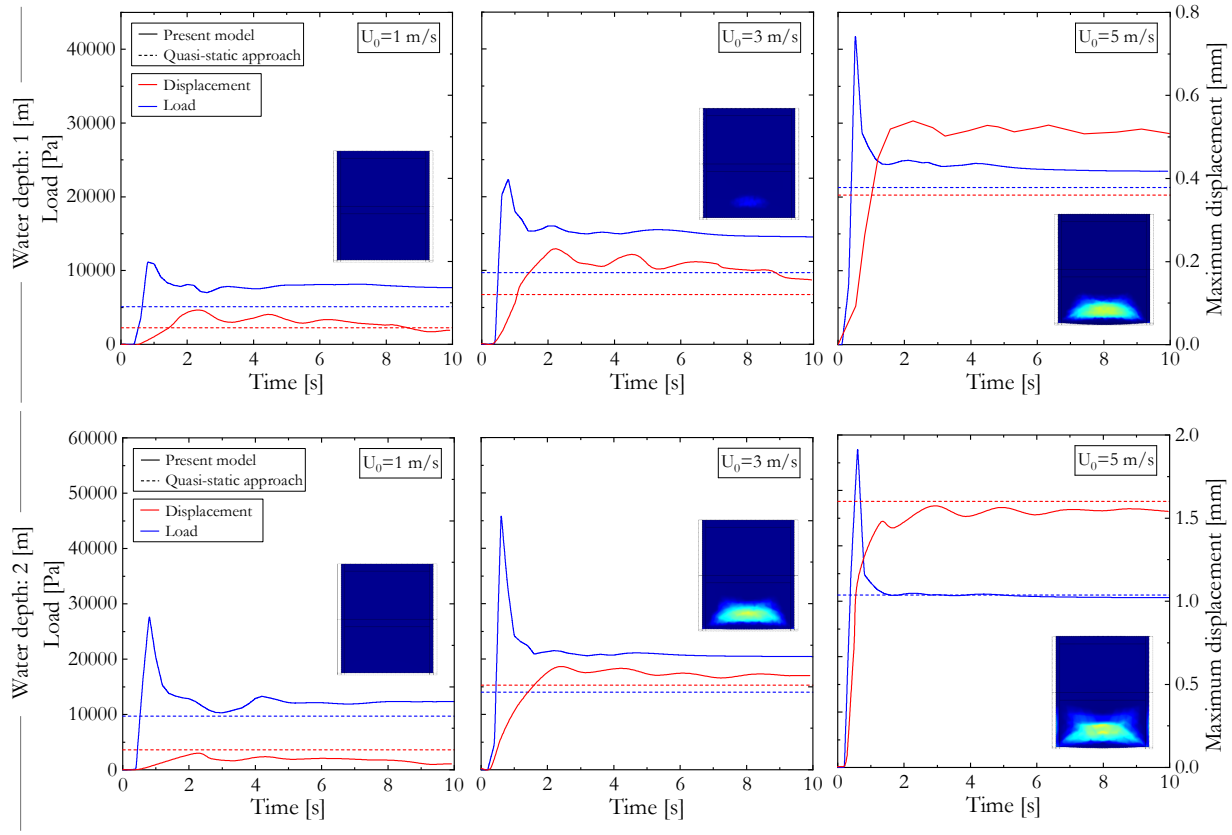

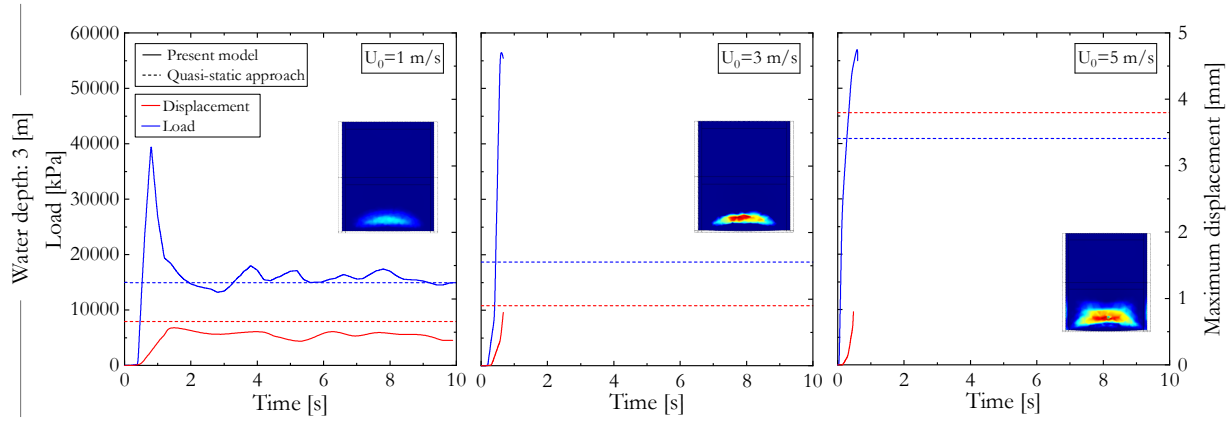

Figure 8: Global structural response obtained by the multilevel model by varying water depth and inlet velocity.

The damage maps reveal the evolution of structural failure. At higher velocities, a more widespread damage pattern is observed, extending toward the edges of the wall, resembling the expected collapse mechanism of a masonry panel under lateral fluid pressure. When both high water depths and velocities are combined ($H^w = 3$ m and $U_0 = 3$ m/s , $U_0 = 5$ m/s), the structure collapses, indicating that the load-carrying capacity is exceeded under extreme hydrodynamic conditions. Overall, this parametric study confirms that fluid velocity plays a dominant role in determining peak structural loads, while water depth influences the extent of damage and the collapse mechanism. The results emphasize the limitations of quasi-static methods in capturing the actual fluid-induced response, reinforcing the necessity of dynamic modeling for accurate structural assessment under extreme loading conditions.

CONCLUSIONS

This study presents a novel 3D multilevel numerical framework to analyze the structural response of masonry buildings under flash flood-induced loading conditions. An integrated approach, that combines a macro-scale fluid model using computational fluid dynamics with a meso-scale structural model, which employs a coupled damage-plasticity formulation for masonry material behavior analysis, is developed.

The integrated model was employed to assess the fluid-structure interaction effects on the global structural response of a real-scale masonry structure subjected to flood-induced load, in terms of load-carrying capacity and damage patterns. The results show that the proposed multilevel framework provides accurate and reliable predictions in fluid pressure distributions, structural deformations, and damage patterns. A comparison with an available quasi-static approach highlights that dynamic effects must be included to accurately determine peak load and damage distribution. As a matter of fact, the quasi-static model underestimates both load and structural out-of-plane displacement of about 10% and 28%, respectively. The work includes a parametric analysis that evaluates how structural response varies with changes in water depth and fluid velocity. The results show that fluid velocity primarily controls peak load values while water depth affects both damage extension and failure mechanisms. In extreme conditions, high-velocity and high-depth flood events lead to structural collapse, confirming the critical role of hydrodynamic forces in the failure of masonry buildings.

While certain simplifications have been adopted, such as the use of a homogeneous material representation for masonry and the neglect of specific local effects (e.g., material degradation due to water exposure, possible sliding between masonry units), the multilevel framework provides a robust basis for vulnerability assessments of masonry buildings exposed to flash floods. Future developments will focus on refining the modeling of material heterogeneities and local mechanisms, with the aim of further extending the framework's applicability to a broader range of masonry structures and damage scenarios.

ACKNOWLEDGMENTS

The authors gratefully acknowledge financial support from the Next Generation EU—Italian NRRP, Mission 4, Component 2, Investment 1.5, call for the creation and strengthening of 'Innovation Ecosystems', building

'Territorial R&D Leaders' (Directorial Decree n. 2021/3277)—project Tech4You—Technologies for climate change adaptation and quality of life improvement, n. ECS0000009.

REFERENCES

[1] Drdácký, M.F. (2010). Flood Damage to Historic Buildings and Structures, J. Perform. Constr. Facil., 24(5), pp. 439–445, DOI: 10.1061/(ASCE)CF.1943-5509.0000065.
[2] Tarbotton, C., Dall'Osso, F., Dominey-Howes, D., Goff, J. (2015). The use of empirical vulnerability functions to assess the response of buildings to tsunami impact: Comparative review and summary of best practice, Earth-Science Rev., 142, pp. 120–134, DOI: 10.1016/j.earscirev.2015.01.002.
[3] Zanchetta, G., Sulpizio, R., Pareschi, M.T., Leoni, F.M., Santacroce, R. (2004). Characteristics of May 5–6, 1998 volcaniclastic debris flows in the Sarno area (Campania, southern Italy): relationships to structural damage and hazard zonation, J. Volcanol. Geotherm. Res., 133(1–4), pp. 377–393, DOI: 10.1016/S0377-0273(03)00409-8.
[4] Zhang, J., Tang, H., Tannant, D.D., Lin, C., Xia, D., Wang, Y., Wang, Q. (2021). A Novel Model for Landslide Displacement Prediction Based on EDR Selection and Multi-Swarm Intelligence Optimization Algorithm, Sensors, 21(24), pp. 8352, DOI: 10.3390/s21248352.
[5] Papathoma-Köhle, M., Neuhäuser, B., Ratzinger, K., Wenzel, H., Dominey-Howes, D. (2007). Elements at risk as a framework for assessing the vulnerability of communities to landslides, Nat. Hazards Earth Syst. Sci., 7(6), pp. 765–779, DOI: 10.5194/nhess-7-765-2007.
[6] Wu, X., Wang, Z., Guo, S., Liao, W., Zeng, Z., Chen, X. (2017). Scenario-based projections of future urban inundation within a coupled hydrodynamic model framework: A case study in Dongguan City, China, J. Hydrol., 547, pp. 428–442, DOI: 10.1016/j.jhydrol.2017.02.020.
[7] Mazzorana, B., Simoni, S., Scherer, C., Gems, B., Fuchs, S., Keiler, M. (2014). A physical approach on flood risk vulnerability of buildings, Hydrol. Earth Syst. Sci., 18(9), pp. 3817–3836, DOI: 10.5194/hess-18-3817-2014.
[8] Custer, R., Nishijima, K. (2015). Flood vulnerability assessment of residential buildings by explicit damage process modelling, Nat. Hazards, 78(1), pp. 461–496, DOI: 10.1007/s11069-015-1725-7.
[9] Milanesi, L., Pilotti, M., Belleri, A., Marini, A., Fuchs, S. (2018). Vulnerability to Flash Floods: A Simplified Structural Model for Masonry Buildings, Water Resour. Res., 54(10), pp. 7177–7197, DOI: 10.1029/2018WR022577.
[10] Lonetti, P., Maletta, R. (2018). Dynamic impact analysis of masonry buildings subjected to flood actions, Eng. Struct., 167, pp. 445–458, DOI: 10.1016/j.engstruct.2018.03.076.
[11] De Maio, U., Greco, F., Lonetti, P., Nevone Blasi, P. (2024). A Multiscale Model to Assess Bridge Vulnerability Under Extreme Wave Loading, J. Mar. Sci. Eng., 12(12), pp. 2145, Doi: 10.3390/jmse12122145.
[12] Caporale, A., Feo, L., Luciano, R., Penna, R. (2013). Numerical collapse load of multi-span masonry arch structures with FRP reinforcement, Compos. Part B Eng., 54, pp. 71–84, DOI: 10.1016/j.compositesb.2013.04.042.
[13] Caporale, A., Luciano, R. (2012). Limit analysis of masonry arches with finite compressive strength and externally bonded reinforcement, Compos. Part B Eng., 43(8), pp. 3131–3145, DOI: 10.1016/j.compositesb.2012.04.015.
[14] Caporale, A., Feo, L., Hui, D., Luciano, R. (2014). Debonding of FRP in multi-span masonry arch structures via limit analysis, Compos. Struct., 108, pp. 856–865, DOI: 10.1016/j.compstruct.2013.10.006.
[15] Caporale, A., Feo, L., Luciano, R. (2012). Limit analysis of FRP strengthened masonry arches via nonlinear and linear programming, Compos. Part B Eng., 43(2), pp. 439–446, DOI: 10.1016/j.compositesb.2011.05.019.
[16] Funari, M.F., Spadea, S., Lonetti, P., Fabbrocino, F., Luciano, R. (2020). Visual programming for structural assessment of out-of-plane mechanisms in historic masonry structures, J. Build. Eng., 31, pp. 101425, DOI: 10.1016/j.jobe.2020.101425.
[17] Darban, H., Luciano, R., Caporale, A., Fabbrocino, F. (2020). Higher modes of buckling in shear deformable nanobeams, Int. J. Eng. Sci., 154, pp. 103338, DOI: 10.1016/j.ijengsci.2020.103338.
[18] Luciano, R., Willis, J.R. (2003). Boundary-layer corrections for stress and strain fields in randomly heterogeneous materials, J. Mech. Phys. Solids, 51(6), pp. 1075–1088, DOI: 10.1016/S0022-5096(02)00146-1.
[19] Fang, Q., Liu, S., Zhong, G., Zhang, H., Liang, J., Zhen, Y. (2021). Nonlinear Simulation and Vulnerability Analysis of Masonry Structures Impacted by Flash Floods, Shock Vib., 2021(1), DOI: 10.1155/2021/6682234.
[20] Wilcox, D.C. (1998). Turbulence Modeling for CFD, DCW Industries.
[21] Launder, B.E., Spalding, D.B. (1974). The numerical computation of turbulent flows, Comput. Methods Appl. Mech. Eng., 3(2), pp. 269–289, DOI: 10.1016/0045-7825(74)90029-2.
[22] Grassl, P., Xenos, D., Nyström, U., Rempling, R., Gylltoft, K. (2013). CDPM2: A damage-plasticity approach to modelling the failure of concrete, Int. J. Solids Struct., 50(24), pp. 3805–3816, DOI: 10.1016/j.ijsolstr.2013.07.008.

[23] De Maio, U., Greco, F., Nevone Blasi, P., Pranno, A., Sgambitterra, G. (2024). Elastic Wave Propagation Control in Porous and Finitely Deformed Locally Resonant Nacre-like Metamaterials, Materials (Basel)., 17(3), pp. 705, DOI: 10.3390/ma17030705.

[24] De Maio, U., Gaetano, D., Greco, F., Luciano, R., Pranno, A. (2024). Degradation analysis of dynamic properties for plain concrete structures under mixed-mode fracture conditions via an improved cohesive crack approach, Frat. Ed Integrità Strutt., 18(68), pp. 422–439, DOI: 10.3221/IGF-ESIS.68.28.

[25] De Maio, U., Gaetano, D., Greco, F., Lonetti, P., Nevone Blasi, P., Pranno, A. (2023). The Reinforcing Effect of Nano-Modified Epoxy Resin on the Failure Behavior of FRP-Plated RC Structures, Buildings, 13(5), pp. 1139, DOI: 10.3390/buildings13051139.